



Düzce University Journal of Science & Technology

Research Article

The Investigation of Electrochemical Corrosion Behaviour of Fe Matrix Composites at Room and Elevated Temperatures

 Fatih AYDIN ^{a,*},  Mehmet Akif ERDEN ^b

^a Department of Metallurgical and Materials Engineering, Faculty of Engineering, Karabük University, Karabük, TURKEY

^b Department of Manufacturing Engineering, Faculty of Technology, Karabük University, Karabük, TURKEY

* Corresponding author's e-mail address: fatih.aydin@karabuk.edu.tr

DOI: 10.29130/dubited.542876

ABSTRACT

In this study, pure Fe and Fe matrix composites (5 wt. % nano- Al_2O_3 , 5 wt. % micron- B_4C and 2.5 wt. % nano- Al_2O_3 -2.5 wt. % micron- B_4C) were manufactured via powder metallurgy. The density and phase analysis of the produced samples were performed. The electrochemical corrosion behaviour of the samples in a 3.5 wt. % NaCl solution was studied using potentiodynamic polarization at 25, 50 and 75 °C. The corrosion rate of the samples significantly increased with increasing test temperature. Also, the effect of reinforcement particulates leads to deteriorate corrosion resistance of pure Fe due to the presence of galvanic reactions.

Keywords: Fe matrix composites, Corrosion, Galvanic reaction, Al_2O_3 , B_4C

Fe Matrisli Kompozitlerin Oda ve Yüksek Sıcaklıklardaki Elektrokimyasal Korozyon Davranışının İncelenmesi

ÖZET

Bu çalışmada, saf Fe ve Fe matrisli kompozitler (% 5ağ. nano- Al_2O_3 , %5ağ. mikron- B_4C ve %2.5 ağ. nano- Al_2O_3 -2.5 ağ. % mikron- B_4C) toz metalurjisi ile üretilmiştir. Üretilen numunelerin yoğunluk ölçümleri ve faz analizleri gerçekleştirilmiştir. Numunelerin elektrokimyasal korozyon davranışı 25, 50 ve 75 °C'de %3.5NaCl çözeltisi içinde potansiyodinamik polarizasyon ile gerçekleştirilmiştir. Numunelerin korozyon hızları artan test sıcaklığıyla önemli ölçüde artmıştır. Ayrıca, takviye partikülleri galvanik reaksiyonlar sebebiyle saf Fe'in korozyon dayanımını kötüleştirmiştir.

Anahtar Kelimeler: Fe matrisli kompozitler, Korozyon, Galvanik reaksiyon, Al_2O_3 , B_4C

I. INTRODUCTION

Metal matrix composites (MMCs) exhibit better wear resistance, structural and mechanical properties compared to conventional metal and alloys [1]. When compared to other MMCs, Fe-MMCs have gained interest especially for wear resistant applications [2]. Different reinforcements such as SiC [3], TiC [4], Al₂O₃ [5], Fe₂O₃ [6], WC [7] were used as reinforcement materials for production of Fe-MMCs. There are different important properties such as mechanical, wear and corrosion, which affects the service life of Fe-MMCs.

There are several studies on wear and mechanical behaviour of Fe-MMCs in the literature. In one of those studies, Gupta et al. have investigated the sintering mechanism on wear behaviour of Fe-Al₂O₃ composites and reported the improved wear resistance for composites in comparison to pure Fe [5]. Vedantam et al. have studied the effect of reinforcement type, size and volume fraction on tribological performance of Fe matrix composites. It was reported that Fe / mullite composites exhibits higher wear performance than Fe/silica composites owing to higher elastic modulus of mullite [8]. In another study, Gupta et al. have examined the sintering and hardness behaviour of Fe-Al₂O₃ nanocomposites by powder metallurgy [9]. Kumar et al. have developed a novel Fe / MWCNT nanocomposite via high energy ball milling. It is reported that good interfacial structure leads to significant improvement of magnetic properties of Fe / 2wt% MWCNT nanocomposites [10]. In another study, Kumar et al. have investigated the effect of MWCNT content (1, 2, 3 and 4 wt.%) on the magnetic, electrical and compression properties of pure Fe. It was observed that increasing MWCNT content leads to increase in compressive strength and electrical conductivity of pure Fe. The 3wt.% MWCNT exhibits the best hardness results in comparison with the other contents of MWCNT [11]. Chen et al. have examined the compression fracture behaviour of Fe / WC composites [12]. Ramya et al. have manufactured Fe / Fe₃O₄ (5, 10 and 15 wt.%) nanocomposites by high energy ball milling. The produced samples were analysed by XRD, SEM and magnetic measurements (hysteresis loops) [13].

To the best of our knowledge, the investigation of corrosion behaviour of Fe-MMCs is quite limited compared to the investigations of mechanical and wear behaviour. In one of those studies, Gupta et al. have examined the effect of sintering parameters on the corrosion behaviour of Fe-Al₂O₃ composites at room temperature by electrochemical test. It was reported that the formation of iron aluminate leads to increase in corrosion resistance of Fe-Al₂O₃ composites [14]. Khosla et al. also have investigated the mechanical and electrochemical corrosion behaviour of Fe-SiC composites. It was reported that Fe / 5wt.% SiC composite that sintered 900°C exhibits the best corrosion performance owing to the presence of Fe₃Si phase in the structure [15]. Jasinska et al. have studied the corrosion behavior of Fe / Mg₂Si composites produced by powder metallurgy. At the end of the study, electrochemical and static immersion test results show that the addition of Mg₂Si deteriorates the corrosion performance of pure Fe [16]. Zhao et al. have investigated the corrosion performance of Fe/Graphene oxide composite produced by selective laser melting. It was reported that the Fe/Graphene oxide composite exhibits higher biodegradation rate than pure Fe [17]. When the literature studies are examined, no study was detected on electrochemical corrosion behaviour of monolithic and hybrid Fe - MMCs at elevated temperatures.

The aim of this study is to research the density, phase analysis and electrochemical corrosion behaviour of unhybrid Fe / B₄C, Fe / Al₂O₃ and hybrid Fe / B₄C (micron)-Al₂O₃ (nano) composites. Firstly, samples were manufactured by powder metallurgy. The density, phase analysis and electrochemical corrosion behaviour of the samples were investigated. Also, the micrographs of the corroded samples were examined by Optical Microscopy.

II. EXPERIMENTAL PROCEDURE

In this study, pure Fe powder (~100 μm), B_4C powder (~40 μm) and Al_2O_3 powder (~50 nm) were used as matrix and reinforcement materials. The powders were mixed using turbulamixer for 3 h. Pure Fe, Fe / 5 wt. % B_4C , Fe / 5 wt. % Al_2O_3 and Fe / 2.5wt. % B_4C - 2.5wt. % Al_2O_3 were compacted under pressure of 500 MPa and sintered at 1050 $^\circ\text{C}$ for 1.5h. Figure 1 shows the produced samples. The samples were about 32 mm in diameter and 10 mm height.

Density measurements were performed using Radwag balance electronic balance (± 0.1 mg accuracy) with distilled water. The phase analysis was carried out on XRD device (Rigaku Ultima IV) with Cu ($\text{K}\alpha$ radiation, $\lambda: 1.54 \text{ \AA}$) tube. Microstructure characterization of the samples was carried out a Scanning Electron Microscopy (SEM, Carl Zeiss Ultra Plus) equipped with an energy-dispersive spectrometer (EDS, Bruker X Flash 6/10).

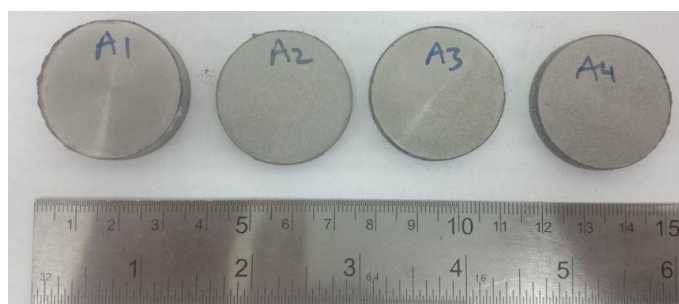


Figure 1. The images of the samples

Electrochemical corrosion tests of the samples were performed in 3.5 wt. % NaCl solution using Parstat 4000 model potentiostat/galvanostat at 25, 50 and 75 $^\circ\text{C}$. Figure 2 shows the image of corrosion test setup. Ag/AgCl₂ electrode was used as reference electrode. The graphite was used as a counter electrode. The interval of - 500 mV and 500 mV was used versus open circuit potentials (OPC). Scanning rate was 1 mV/s. The corroded surfaces of the samples were examined by Optical Microscope. The corrosion samples were grinded with emery papers (from 240 to 2000 mesh) to obtain good surface for corrosion tests. After grinding step, the samples were dried with ethyl alcohol. The surface area of the specimens was about 0.6 cm^2 for corrosion tests.

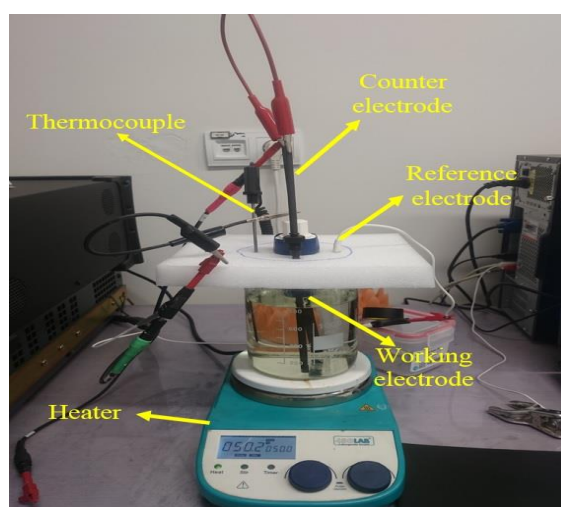


Figure 2. The corrosion test setup

III. RESULTS and DISCUSSION

A. DENSITY AND PHASE CHARACTERIZATION

The density results of the samples is given in Table 1. It can be seen that pure Fe has the highest relative density (94.6%). Also, the addition of reinforcements leads to decrease in relative density for pure Fe. The decrease in relative density with increasing reinforcement content can be attributed to the presence of possible micro-porosities in the composite samples [18].

Table 1. Density results of the samples.

Material	Theoretical density (g/cm ³)	Actual density (g/cm ³)	Relative density %
Pure Fe	7.874	7.450	94.6
Fe / 5 Al ₂ O ₃	7.677	6.950	90.5
Fe / 5 B ₄ C	7.606	6.557	86.2
Fe / 2.5 B ₄ C - 2.5 Al ₂ O ₃	7.641	6.616	86.5

Figure 3 shows the SEM image and EDS analysis of the hybrid Fe / 2.5 B₄C - 2.5 Al₂O₃ composite. In the image, B₄C and Al₂O₃ particulates were indicated by yellow arrows. Also, it can be seen that the general distribution of the particulates is homogenous. EDS analyzes were applied to different areas to verify the presence and location of B₄C and Al₂O₃ particles. The EDS analysis of area 1 shows the significant amount of B (83.7%) and C (15.8%) content. This results verify the presence of B₄C particles. After the EDS analysis of area 2, the high amount of Al (48.1%) and O (49.1%) was detected. This result is the evidence of the presence of Al₂O₃ particles.

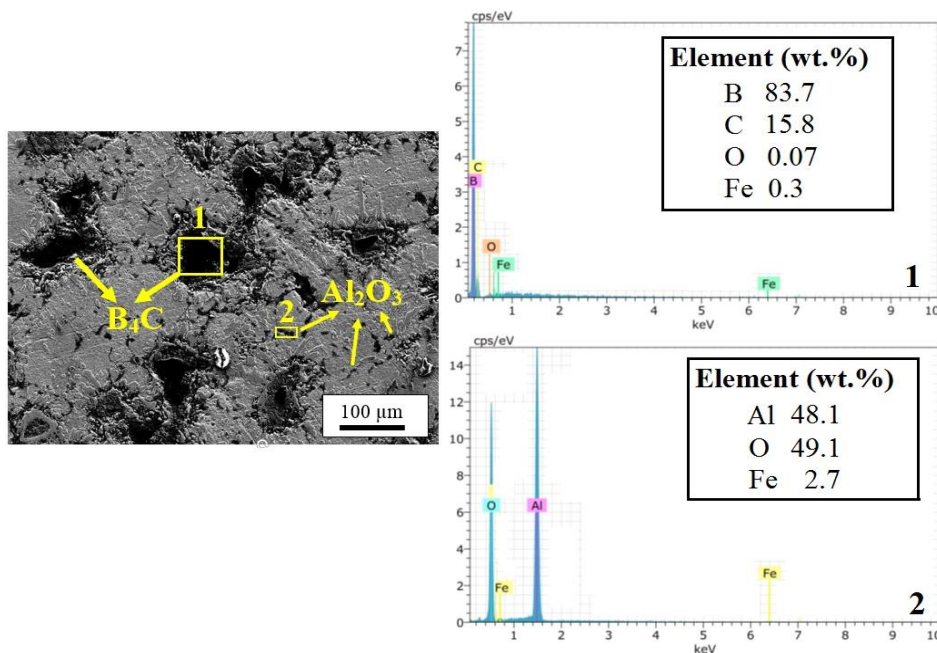


Figure 3. SEM image and EDS analysis of the Fe / 2.5 B₄C - 2.5 Al₂O₃ composite

Figure 4 illustrates the XRD patterns of the samples. For pure Fe, only peaks of Fe were detected. It can be seen that, for Fe / 5 Al₂O₃ composite, both Fe and Al₂O₃ peaks are discernible. It is also worth to say that B₄C and Fe₂B phases are present in the structure of Fe / 5 B₄C and Fe / 2.5 B₄C - 2.5 Al₂O₃. The formation of Fe₂B can be related to the reaction between Fe and B during sintering.

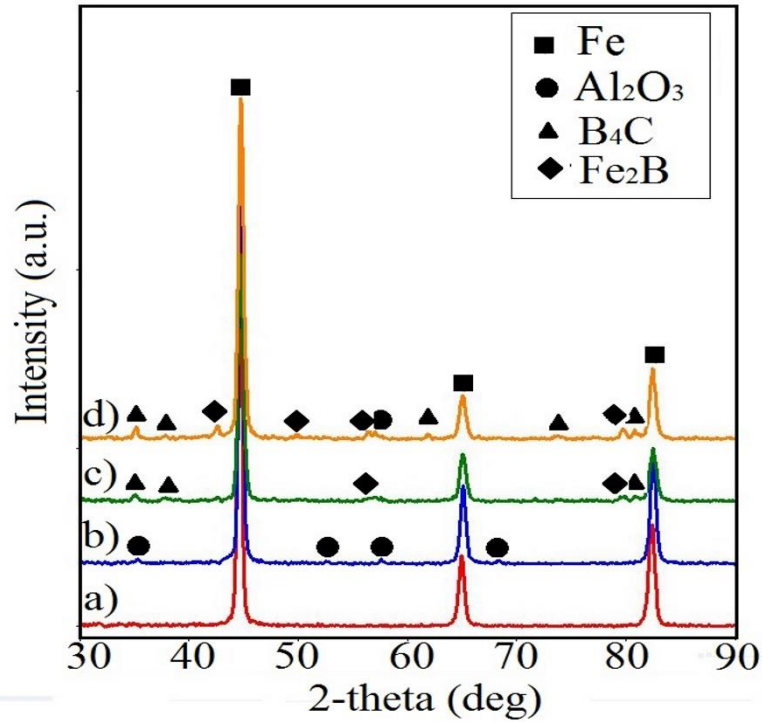


Figure 4. XRD patterns of the a) pure Fe, b) Fe / 5 Al₂O₃, c) Fe / 5 B₄C and d) Fe / 2.5 B₄C - 2.5 Al₂O₃

B. CORROSION TEST RESULTS

Figure 5 represents the potentiodynamic polarization curves for the samples at different temperatures. The corrosion potentials (E_{corr}), corrosion current densities (i_{corr}) and corrosion rate are also calculated by Tafel extrapolation and given in Table 2. The corrosion rate of the samples was calculated according to Eq. 1[19]:

$$\text{Corrosion rate (mm/year)} = \lambda \cdot i_{\text{corr}} \cdot (\text{E.W.}) / d \quad (1)$$

Where;

$\lambda = 3.27 \times 10^{-3} (\text{mm} \cdot \text{g}) / (\text{mA} \cdot \text{cm} \cdot \text{year})$ is a metric conversion factor

E.W=Equivalent weight

d=Density (g/cm^3)

It can be seen from the Fig. 5, Tafel slopes of the samples are nearly similar for all samples under different temperatures. This can be the result of similar corrosion mechanism for the samples. After the addition of reinforcement particles, the potential (E_{corr}) shows the lower values in comparison with pure Fe. This is related to the more active behaviour of the Fe matrix due to the presence of reinforcement elements [16]. At the same time, the increasing test temperature leads to more negative potential values for all samples. For example, the E_{corr} values for pure Fe at 25, 50 and 75 °C, was calculated as -464.4, -634.4 and -715.8 mV, respectively. Pure Fe is converted to Fe^{+2} ions and two free electrons in solution. These electrons combine with proton to form H_2 gas. As a result, H_2 gas emerges as bubbles in solution [15].

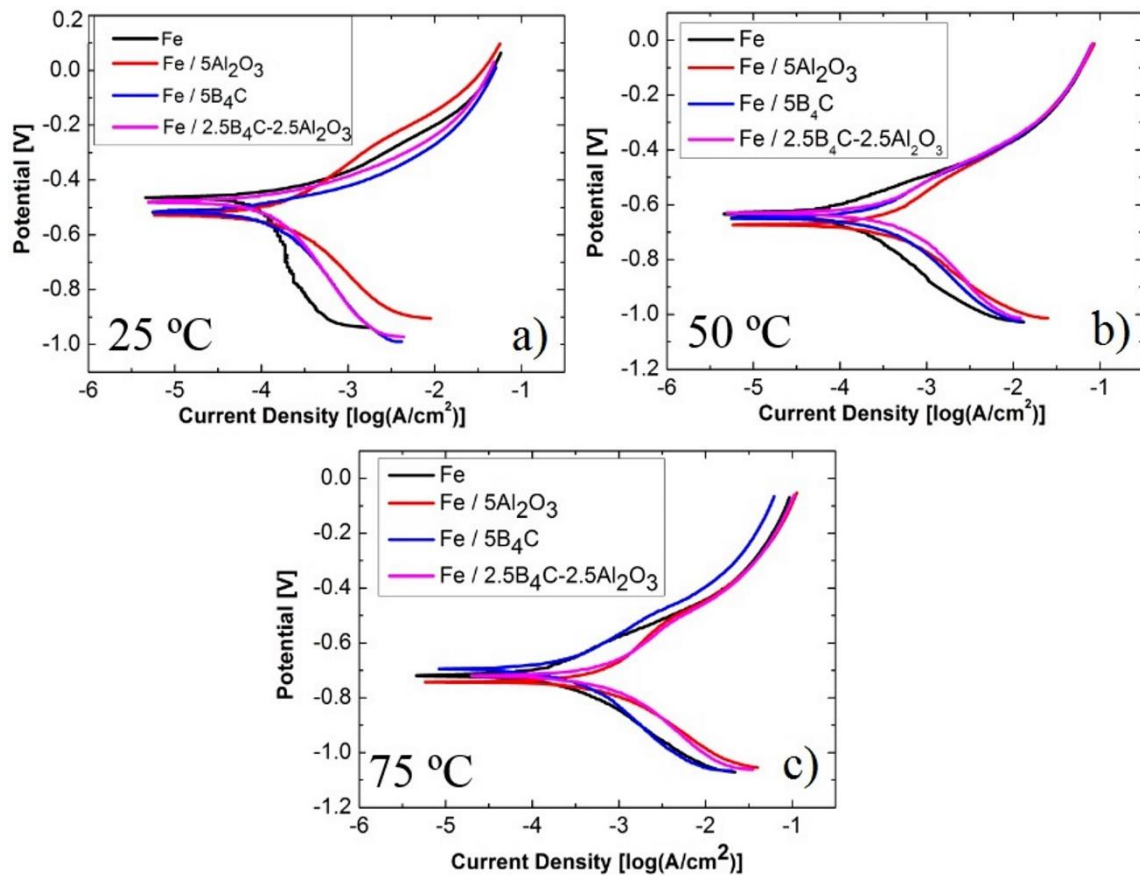


Figure 5. Potentiodynamic curves of the samples at a) 20 °C, b) 50 °C and c) 75 °C

From the Table 2, it is clear that pure Fe has the highest corrosion resistance (the lowest corrosion rate) at all temperatures. It is reported that the corrosion rate of the pure Fe at 25, 50, 75 °C is 0.9, 1.0 and 1.4 mm/year, respectively. All composite materials exhibits higher corrosion rate compared to pure Fe. Also, the increase in test temperature give rise to significant deterioration for composite materials. At the temperature of 25 °C, Fe / 5Al₂O₃ has the highest corrosion rate (3.1 mm/year). However, hybrid Fe / 2.5 B₄C - 2.5Al₂O₃ composite has the highest corrosion rate among the all samples (14.2 mm/year). The higher corrosion rates of the composites can be related to the localized attack at the matrix-particle interface. Also, the cathodic sites with increasing reinforcement content in the matrix is presence in the structure. The smaller anodic area sustains high current density resulting in higher corrosion rate [1].

Cheng et al. have investigated the corrosion behaviour of Fe-Fe₂O₃ (2, 5, 10, and 50 wt.%) composites produced by spark plasma sintering. It was reported that the addition of Fe₂O₃ accelerates the corrosion rate of pure Fe (except for 10 wt.% Fe₂O₃ content) according to electrochemical corrosion tests. It was concluded that there is a galvanic corrosion reaction between grain and phase boundaries. It is also reported that the addition of Fe₂O₃ particles give rise to increase in amount of phase boundaries and active sites. The effect of reinforcement particles (B₄C and Al₂O₃) on corrosion rate on pure Fe can be evaluated in different aspects. One of them, the addition of reinforcement particles lead to significant increase in structural defects. The second one, uniform dispersion and presence of second phase in grain boundaries can acts a barrier to electron transfer from matrix to grains. At the end of this, corrosion rate decreased in comparison with pure Fe [6].

Jasinska et al. have studied the corrosion behaviour Fe / Mg₂Si (1 wt.%) composite produced by powder metallurgy. The corrosion rate of pure Fe and Fe/ Mg₂Si composite was reported as 0.26 and 0.41 mm/year, respectively. The corrosion mechanism is explained by preferential anodic dissolution

of Mg in Mg₂Si particles. It is also reported that there is a micro-galvanic effects between local anodes (Mg₂Si) and cathodes (Fe matrix) [16].

Gupta et al. have examined the effect of sintering parameters on corrosion performance of Fe / Al₂O₃ composites. It was reported that the addition of Al₂O₃ particles give rise to increase corrosion resistance of pure Fe. This situation was associated with to the formation nano iron aluminate phase on the surface of Fe. The formation of iron aluminates decreased wettability and reduces the surface roughness [14].

Table 2. Corrosion results of the samples

Materials	E _{corr} (mV)	β _a (mV)	β _c (mV)	i _{corr} (μA)	C.R. (mm/year)
Fe - 25 °C	-464.4	291.4	108.8	50.1	0.9±0.08
Fe - 50 °C	-634.4	131.2	230.6	65.0	1.0±0.07
Fe - 75 °C	-715.8	148.1	136.0	89.1	1.4±0.08
Fe / 5Al ₂ O ₃ - 25 °C	-523.4	289.1	349.4	133.3	3.1±0.34
Fe / 5Al ₂ O ₃ - 50 °C	-673.0	390.1	282.3	289.3	6.6±0.53
Fe / 5Al ₂ O ₃ - 75 °C	-741.7	392.0	210.3	480.3	11.4±1.21
Fe / B ₄ C - 25 °C	-512.6	106.3	363.7	69.5	1.6±0.06
Fe / B ₄ C - 50 °C	-644.6	200.9	222.8	149.2	3.5±0.21
Fe / B ₄ C - 75 °C	-697.9	201.0	258.4	163.6	3.9±0.23
Fe / 2.5 B ₄ C- 2.5Al ₂ O ₃ - 25°C	-482.1	106.0	399.2	79.5	1.4±0.05
Fe / 2.5 B ₄ C- 2.5Al ₂ O ₃ - 50°C	-634.0	195.1	273.4	191,5	4.0±0.57
Fe / 2.5 B ₄ C - 2.5Al ₂ O ₃ - 75°C	-720.3	331.6	301.1	667.9	14.2±1.32

Figure 6 a-c-e-g shows the optical micrographs of the corroded samples at 25 °C. In the figures, corroded and un-corroded area of the samples were indicated with red arrows. From the Fig. 6a-c-e-g, it is clear that pure Fe has the highest fresh and un-corroded area. It is seen that local corrosion can be seen for pure Fe at 25 °C. It is also possible to say that some corrosion pits are present for pure Fe.

Even if pitting corrosion was observed for pure Fe, anodic slope of Tafel plots (in Fig 5.a) shows no presence of pitting corrosion. In the literature studies, Jasinska et al. reported the presence of pitting corrosion by corroded images of the surface and potentiodynamic curves [16]. In an another study, Cheng et al have verified the presence of pitting corrosion for pure Fe after polarization test. However, potentiodynamic polarization curves don't shows the starting of pitting corrosion for their study. The deeper holes were observed with increasing reinforcement content (Fe₂O₃) [6].

It is clearly seen that the area of corroded surfaces of the composite materials significantly increased. Fe / 5Al₂O₃ composite has the highest corroded area compared to other samples (Fig6.c). Also, it is concluded that composite materials suffer from severe corrosion for both 25 and 75 °C. It is well known that the size and distribution of reinforcement particles significantly affects the corrosion properties and mechanism for Fe matrix composites. The severe corrosion for composite materials can be attributed to the micro-galvanic corrosion between reinforcement particles and Fe matrix. The micro-galvanic corrosion generally give rise to more aggressive dissolution of the composite surfaces in comparison with pure Fe sample [16].

Figure 6 b-d-f-h illustrates the optical micrographs of the corroded samples at 75 °C. For pure Fe, the main corrosion mechanism can be identified as grain boundary corrosion. Jasinska et al. have reported the presence of grain boundary corrosion for pure Fe after static immersion tests [16]. In an another study, the grain boundary corrosion was observed for pure Fe after immersion tests [6]. It is observed that the increasing test temperature (from 25 °C to 75 °C) led to significant amount of surface degradation (Fig. 6 b-d-f-h). It is clearly seen that increasing solution temperature causes severe surface damage for both pure Fe and its composites. However, the damage of composite materials is higher than that of pure Fe. Zakaria has investigated the corrosion behaviour of Al/SiC composites by

static immersion tests at 25, 50 and 75 °C. It was reported that corrosion rate of Al/SiC composites increased with increasing test temperature [20]. Generally, the effect of temperature on the corrosion rate depends on two factors: the energy of activation of corrosion and the temperature variation of the corrosion gradient. It is well known that corrosion rate increases with activation energy due to increase in permeation rate [21].

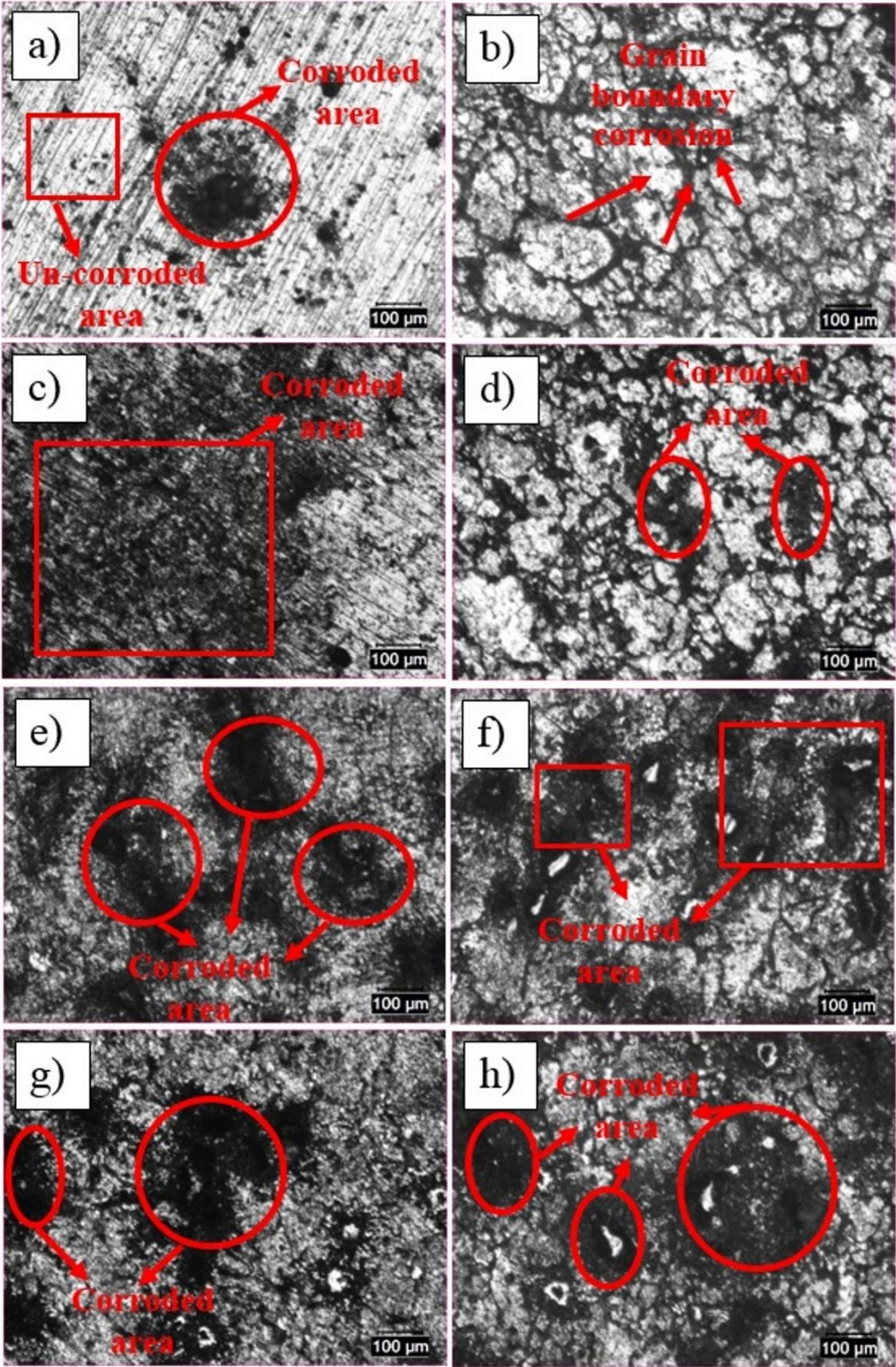


Figure 6. Optical micrographs of the corroded samples at 25 °C, a) pure Fe, c) Fe / 5 Al₂O₃, e) Fe / 5 B₄C and g) Fe / 2.5 B₄C - 2.5 Al₂O₃, at 75 °C b) pure Fe, d) Fe / 5 Al₂O₃, f) Fe / 5 B₄C and h) Fe / 2.5 B₄C - 2.5 Al₂O₃

IV. CONCLUSION

In this study, pure Fe, Fe / 5 Al₂O₃ (nano), Fe / 5 B₄C (micron) and Fe 2.5 Al₂O₃-2.5 B₄C (nano-micron) samples were successfully manufactured by powder metallurgy. The relative densities of the composites is lower than that of pure Fe. Electrochemical corrosion tests show that pure Fe has the lowest corrosion rate among all samples. Also, the corrosion rate of the samples significantly increased with increasing test temperature. The higher corrosion rate of the composite is attributed to the presence anodic and cathodic sites in the structure which lead to galvanic interaction.

V. REFERENCES

- [1] A. K. Srivastava, K. Das and S. K. Toor, "Corrosion behaviour of TiC-Reinforced hadfield manganese austenitic steel matrix In-Situ composites," *Open Journal of Metals*, vol. 5, pp. 11-17, 2015.
- [2] K. Das, T. K. Bandyopadhyay and S. Das, "A review on the various synthesis routed of TiC reinforced ferrous based composites," *Journal of Materials Science*, vol. 37, no. 18, pp. 3881-3892, 2002.
- [3] J. Pelleg, "Reactions in the matrix and interface of the Fe-SiC metal matrix composite system," *Materials Science and Engineering A*, vol. 269, no.1-2, pp. 225-241, 1999.
- [4] W. Jing and W. Yisan, "In-situ production of Fe-TiC composite," *Materials Letters*, vol. 61, no. 22, pp. 4393-4395, 2007.
- [5] P. Gupta, D. Kumar, O. Parkash, A.K. Jha and K.K. Sadasivuni, "Dependence of wear behavior on sintering mechanism for Iron- alumina metal matrix nanocomposites," *Materials Chemistry and Physics*, vol. 220, pp. 441-448, 2018.
- [6] J. Cheng, T. Huang and Y.F. Zheng, "Microstructure, mechanical property, biodegradation behavior, and biocompatibility of biodegradable Fe-Fe₂O₃ composites," *Journal of Biomedical Materials Research Part A*, vol. 102, no. 7, pp. 2277-2287, 2014.
- [7] D. Liu, L. Li, F. Li and Y. Chen, "WCp/Fe metal matrix composites produced by laser melt injection," *Surface & Coatings Technology*, vol.202, no. 9, pp. 1771-1777, 2008.
- [8] T. R. Prabhu, V. K.Varma and S. Vedantam, "Effect of reinforcement type, size, and volume fraction on the tribological behavior of Fe matrix composites at high sliding speed conditions," *Wear*, vol. 309, no. 1-2, pp. 247-255, 2014.
- [9] P. Gupta, D. Kumar, O. Parkash, and A.K. Jha, "Sintering and hardness behavior of Fe-Al₂O₃ metal matrix nanocomposites prepared by powder metallurgy," *Journal of Composites*, vol. 2014, pp.1-10, 2014.
- [10] A. Kumar, M.K. Banerjee, and U. Pandel, "Development of a novel MWCNT reinforced iron matrix nanocomposite through powder metallurgy route," *Powder Technology*, vol. 331, pp. 41-51, 2018.
- [11] A. Kumar, U. Banerjee, M. K. Chowrasia, H. Shekhar, and M.K. Banerjee, "Effect of MWCNT Content on the structure and properties of spark plasma-sintered Iron-MWCNT composites synthesized by high-energy ball milling," *Journal of Materials Engineering and Performance*, vol.28, no. 5, pp. 2983-3000, 2019.

- [12] F. Chen, Z. Li, Q. Shan, Y. Jiang, Y. Zhang, and F. Zhang, "Effects of different matrix on interface and compression fracture behavior of WC particles reinforced iron matrix composites," *Materials Science Forum*, vol. 913, pp. 480-489, 2018.
- [13] V. Ramya, A. Gangwar, S.K. Shaw, N.K. Mukhopadhyay and N.K. Prasad, "Fe/Fe₃O₄ nanocomposite powders with giant high magnetization values by high energy ball milling," *Bulletin of Materials Science*, vol. 42, no. 93, pp. 1-7, 2019.
- [14] P. Gupta, D. Kumar, M.A. Quraishi and O. Parkash, "Effect of sintering parameters on the corrosion characteristics of Iron-Alumina metal matrix nanocomposites," *Journal of Materials and Environmental Science*, vol. 6, no. 1, pp. 155-167, 2015.
- [15] P. Khosla, H. K Singh, V. Katoch, A. Dubey, N. Singh, D. Kumar and P. Gupta, "Synthesis, mechanical and corrosion behaviour of iron-silicon carbide metal matrix nanocomposites," *Journal of Composite Materials*, vol. 52, no. 1, pp. 91-107, 2018.
- [16] M.S. Jasinska, P. Chevallier, S. Turgeon, C. Paternoster, E. Mostaed, M. Vedani, and D. Mantovania, "Understanding the effect of the reinforcement addition on corrosion behavior of Fe/Mg₂Si composites for biodegradable implant applications," *Materials Chemistry and Physics*, vol. 223, pp. 771-778, 2019.
- [17] Y.C. Zhao, Y. Tang, M.C. Zhao, L. Liu, C. Gao, C. Shuai, R.C. Zeng, A. Atrens, and Y. Lin, "Graphene oxide reinforced iron matrix composite with enhanced biodegradation rate prepared by selective laser melting," *Advanced Engineering Materials*, vol. 21, no. 8, pp. 1-5, 2019.
- [18] F. Aydin and Y. Sun, "Investigation of wear behaviour and microstructure of hot-pressed TiB₂ particulate-reinforced magnesium matrix composites," *Canadian Metallurgical Quarterly*, vol. 57, no. 4, pp. 455-469, 2018.
- [19] A. Standard, Standard practice for calculation of corrosion rates and related information from electrochemical measurements, Annu. Book ASTM Stand. ASTM Int. West Conshohocken PA 3 (1994) G102-G89.
- [20] H.M. Zakaria, "Microstructural and corrosion behavior of Al/SiC metal matrix composites," *Ain Shams Engineering Journal*, vol. 5, no. 3, pp. 831-838, 2014.
- [21] S.C. Sharma, "A study on stress corrosion behavior of Al6061/albite composite in higher temperature acidic medium using autoclave," *Corrosion Science*, vol. 43, no. 10, pp. 1877-1889, 2001.